Unlocking enhanced hydrogen evolution with bimetal-organic framework: A synergistic approach

Chhatan Das,[a] Pappu Naskar,[b] Anjan Banerjee,*[b] Sourav Laha,*[c] Moumita Mukherjee,[d] Ayan Datta*[d] and Partha Mahata,*[a]

[a]Department of Chemistry, Jadavpur University, Jadavpur, Kolkata-700 032, West Bengal, India.

Email: parthachem@gmail.com

[b]Department of Chemistry, Presidency University, *86/1, College Street,* Kolkata-700073, West Bengal, India.

Email: anjan.chem@presiuniv.ac.in

[c]Department of Chemistry, National Institute of Technology Durgapur, Mahatma Gandhi Avenue, Durgapur, West Bengal 713209, India.

Email: slaha.ch@nitdgp.ac.in

[d]School of Chemical Sciences, Indian Assocation for the cultivation of Sciences Kolkata, Jadavpur, West Bengal 700032, India,

Email: *spad@iacs.res.in*

ELECTRONIC SUPPLEMENTARY INFORMATION

Table S1. MOF-based electrocatalysts for HER.

Catalyst	**Electrolyte**	**Overpotential [mV] @ 10 mA cm^{-2}**	**Tafel slope [mV dec^{-1}]**	**Stability tests**	**References**
NENU-500	0.5 M H_2SO_4	237	96	2000 CV cycles	[1]
NENU-501	0.5 M H_2SO_4	392	137	2000 CV cycles	
THTA-Co	0.5 M H_2SO_4	283	71	300 CV cycles and Chronopotentiometry for 4 h @ 10 mA cm^{-2}, 34 mV increase	[2]
THTNi$_2$DSP	0.5 M H_2SO_4	333	81	N/A	[3]
CTGU-5	0.5 M H_2SO_4	388	125	Chronopotentiometry for 96 h at 10 mA cm^{-2}.	[4]
CTGU-6	0.5 M H_2SO_4	425	176		
HUST-200	0.5 M H_2SO_4	131	51	2000 CV cycles and Chronopotentiometry for 9 h @ 10 mA cm^{-2}.	[5]
HUST-201	0.5 M H_2SO_4	192	79	2000 cv cycles and Chronopotentiometry for 9	

				h @ 10 mA cm^{-2}, slight decay.	
NU-1000-Ni-S	0.1 M HCl	238	120	Chronopotentiometry for 2 h @ 10 mA cm^{-2}	[6]
$Ni_3(Ni_3{\cdot}HAHATN)_2$	0.1 M KOH	115	45	1000 CV cycles	[7]
$Ni_3(Cu_3{\cdot}HAHATN)_2$		207	102		
$Ni_3(Co_3{\cdot}HAHATN)_2$		162	98		
$Cu_3(Cu_3{\cdot}HAHATN)$		230	112		
3D NibpyfcdHp	0.5 M H_2SO_4 $DMFH^+$	350	60	10000 CV cycles; Chronopotentiometry for 30 h @ 7 mA cm^{-2}	[8]
3D CobpyfcdHp	0.5 M H_2SO_4 $DMFH^+$	400	65	2000 CV cycles	
1D Co(fcdHp)	[$DMF(H^+)$] in CH_3CN	340	110	1000 CV cycles	[9]
	0.5 M H_2SO_4	450	120	1000 CV cycles	
1D Zn(fcdHp)	0.5 M H_2SO_4	340	110	1000 CV cycles	
UU-100(Co)	$NaClO_4$ (0.1 M)/acetate buffer, pH 4	150	250	Chronopotentiometry for 18 h @ 1.7	[10]

				mA cm^{-2}	
(MOS-1)	0.05 M H_2SO_4	340	NA	Chronopotentiometry for 10 h @ 10 mA cm^{-2}	[11]
(MOS-2)	0.05 M H_2SO_4	530	NA		
Hf_{12}-CoDBP/CNTs	0.026 M TFA	650	178	10000 CV cycles, Chronoamperometry for 18 h @ 715 mV overpotential	[12]
2D MOF,$Cu_6(C_8H_4O_4)_6(H_2O)_6 \cdot H_3[P(W_3O_{10})_4]$	0.5 M H_2SO_4	660	100	-	[13]
Cu-MOF: HKUST-1 ED	0.5 M H_2SO_4	590	183.6	Chronopotentiometry for 12 h @ 10 mA cm^{-2}	[14]
HKUST-1 HT	0.5 M H_2SO_4	660	222.4	-	
UiO-66-NH_2-Mo-5	0.5 M H_2SO_4	200	59	5000 CV Cycles, Chronopotentiometry for 7 h @ 10 mA cm^{-2}	[15]
MoCx	0.5 M H_2SO_4	142	53	Chronopotentiometry for 10 h @ 10 mA cm^{-2}	[16]

$Cu_{0.19}Ni_{0.81}$-NKU-101	0.5 M H_2SO_4	324	131	Chronopotentiometry for 24 h @ 10 mA cm^{-2}	[17]
Cu[Ni(2,3-pyrazinedithiolate)$_2$]	pH 1.3 H_2SO_4	530	69	Chronopotentiometry for 4 h @ 10 mA cm^{-2}	[18]
Ni-MOF NiCo-MOF	0.5 M H_2SO_4	150 120	51 39	1000 CV cycles @ 100 mV s^{-1} and Chronoamperometry @ -0.12 V *vs*. RHE for 20 h	This work

Materials

The chemicals required for the synthesis of compound Ni-MOF and NiCo-MOF, $Ni(CH_3CO_2)_2.4H_2O$ (Loba-Chemie, 98%), N- Nicotinoyl Glycine (TCI, >98%), and $Co(CH_3CO_2)_2.4H_2O$ (Sigma-Aldrich, ≥98%) were used as received. The chemicals used for the electrochemical measurements were DMF (99%, Merck), and PVDF (Merck) used as received without further purification. The water used was double distilled.

Synthesis of Ni-MOF

The Ni-MOF was synthesized using the hydrothermal method. A solution was prepared by dissolving 0.5 mM (0.1269 g) of $Ni(CH_3CO_2)_2.4H_2O$ and 0.5 mM (0.0919 g) of N-nicotinoyl

glycine (N-NG) in 5 mL of distilled water. The mixture was homogenized for 30 min at room temperature. Following homogenization, the solution was sealed in a 23 mL PTFE-lined stainless-steel autoclave and heated at 140 °C for 72 h. The resulting product appeared as light green-coloured block-shaped crystals. The crystals were filtered, washed with deionized water under vacuum, and dried under ambient conditions, yielding 75% based on the metal. The calculated elemental analysis for $C_{26}H_{21}N_5O_{10}$ was as follows: C, 45.82%; H, 3.08%; N, 10.28%. The found values after analysis were C, 45.78%; H, 3.02%; N, 10.36%.

Synthesis of NiCo-MOF. The synthesis method similar to that employed for Ni-MOF was utilized, with a modification in the metal precursors. Equal amounts of $Co(CH_3CO_2)_2.\ 4H_2O$ and $Ni(CH_3CO_2)_2.\ 4H_2O$ were dissolved in a 1:1 ratio (0.25 mM each, totalling 0.0635 g for $Co(CH_3CO_2)_2$ and 0.0634 g for $Ni(CH_3CO_2)_2$ in 5 mL of distilled water. The final product consisted of purple-colored crystals. After this period, the crystals were filtered, washed with deionized water under vacuum, and then dried under ambient conditions.

Physical Characterization

The Powder X-ray diffraction (PXRD) pattern of a finely ground sample was recorded using a Bruker D8 Advance X-ray diffractometer, employing Cu Kα radiation with a wavelength (λ) of 1.5418 Å. The experiment covered the 2θ range of 5-50° and was carried out at 40 kV and 40 mA. The Fourier Transform Infrared (FT-IR) spectra were carefully obtained with the Nicolet Magna IR 750 series-II instrument, spanning a broad range from 450 to 4000 cm^{-1}. Thermogravimetric analysis (TGA) were carried out on a Perkin-Elmer instrument STA 6000 under a nitrogen atmosphere (flow rate = 20 mL min^{-1}) in the temperature range 30 – 800 °C (heating rate 10°C min^{-1}). The gas sorption isotherm for nitrogen (77 K) was accurately measured over the pressure range of 0 to 1 bar, employing an Autosorb iQ instrument from

Quantachrome Inc., USA. FE-SEM experiment were carried out using a Zeiss Gemini SEM 450 field emission scanning electron microscope. The metal content in NiCo-MOF was determined using a Thermo Fisher Scientific (Model: iCAP PRO XP Duo) inductively coupled plasma-optical emission spectroscope (ICP-OES) equipped with an Anton Paar, Multiwave 5000 182 microwave digester. Prior to the analysis, 12 mg of samples were dissolved in 2 mL of concentrated HNO_3 and stirred for 1 h at 220 ºC. After digestion, the mixture was filtered by syringe filters having 0.2 μm pore size and the filtrate was diluted before using for the analyses.

Electrochemical Characterizations

The electrocatalytic activities of Ni-MOF and NiCo-MOF towards HER were evaluated through Cyclic Voltammetry (CV), Linear Sweep Voltammetry (LSV), Electrochemical Impedance Spectroscopy (EIS) and chronoamperometry in 3-electrode electrochemical cell configurations. The 3-electrode electrochemical cells were assembled by catalyst (Ni-MOF and NiCo-MOF) coated glassy carbon working electrodes, Pt foil counter electrodes and Ag/AgCl reference electrodes (+0.197 V *vs*. Standard Hydrogen Electrode/SHE) in 0.5 M H_2SO_4 (aq.) electrolyte medium. The electrolyte solution became N_2-saturated by bubbling N_2 gas for 30 min duration. The glassy carbon electrodes (geometric area: 0.2 cm^2) were mechanically polished with a 0.05 μm alumina powder, and followed by washed with ethanol and deionized water for obtaining clean surfaces. The working electrodes were prepared by the drop-casting of catalyst slurries onto the glassy carbon electrodes. The homogeneous catalyst slurries were prepared in N, N-dimethylformamide (DMF) solvent by mixing 90% catalyst and 10% polyvinylidene fluoride (PVDF) binder under the sonication for 30 min. The prepared catalyst-coated working electrodes were dried at 60 ºC for 3 h in hot air oven. The ~ 20 μg (100 μg cm^{-2}) of catalyst loadings were obtained in above mentioned working electrodes. The electrochemical measurements were

acquired in multichannel Autolab potentiostat & galvanostat (Model: M204) at ambient temperature (25 ºC), and the resulting data were presented after iR-compensation. The following equation was applied for the iR-corrections.[19]

$E_{corrected}$ (*vs*. Ag/AgCl) = $E_{experimental}$ (*vs*. Ag/AgCl) - iR_s ……..……. (1)

Whereas, the $E_{corrected}$, $E_{experimental}$, i and R_s are iR-corrected potential, experimental potential, current response and solution resistance obtained from the EIS studies, respectively. However, the iR-corrected potential (E) values were reported with respect to Reversible Hydrogen Electrode (RHE) by using the following pH-dependent relationships.[20]

E (*vs*. RHE) = E (*vs*. SHE) + 0.059×pH ……...…… (2)

E (*vs*. RHE) = E (*vs*. Ag/AgCl) + 0.197 + 0.059×pH …… (3)

The relationship between overpotential (η in V) and current density (j in A cm^{-2}) is depicted in the following Tafel equation[21].

η = a + b×log (j)…….……. (4)

whereas 'a' is the intercept related to the exchange current density (j_0), which indicates the intrinsic electron transfer rate, and 'b' is the Tafel slope that signifies the rate of the electrode process.

The ECSA and RF are calculated as per the following Eqs.

$$ECSA = \frac{Double\ layer\ capacitance\ of\ the\ electrode\ with\ catalyst\ loading\ (Cdl)}{Double\ layer\ capacitance\ of\ the\ blank\ electrode\ without\ catalyst\ loading\ (Cs)} \quad \text{……...} \quad (5)$$

$$RF = \frac{ECSA}{Geometric\ surface\ area\ of\ electrode} \quad \text{.....(6)}$$

The double layer capacitances of the electrodes are estimated from the variable scan rate (υ) CV experiments within the voltage limit of the non-Faradaic electrochemical responses. Herein, the CV profiles under multiple scan rates (υ: 10-100 mV s^{-1}; Δυ = 10 mV s^{-1}) are shown in Fig. S16 (a and c) within 0-0.2 V *vs*. Ag/AgCl for Ni-MOF and NiCo-MOF, respectively. The Fig. S16 (b and d) demonstrate linear profiles of Δj/2 *vs*. υ (Δj = j_{anodic} - $j_{cathodic}$), and the resulting slopes are the measure of the respective double layer capacitance (C_{dl}) of the Ni-MOF and NiCo-MOF electrodes. The double layer capacitance (C_s) of the blank electrode is also estimated by using the similar relationships, while the cyclic voltammograms and Δj/2 *vs*. υ profiles are presented in Fig. S17. Based on the estimated values of C_{dl} and $C_{S.}$

$$\eta\ (V) = [E\ (vs.\ Ag/AgCl) + 0.197 + (0.059 \times pH) - 0] \quad \text{..... (7)}$$

$$TOF\ (s^{-1}) = \frac{j \times A}{2 \times F \times n} \quad \text{..... (8)}$$

Whereas, j is the experimental current density at fixed overpotential, A is the geometric surface area of the catalyst layer, the number 2 indicates requirement of 2 electrons to obtain 1 mole of hydrogen, F is Faraday's constant (96485.3 C mol^{-1}) and n is the mole of catalyst present on the electrode surface. However, the n is calculated from the mass and molecular weight of the catalyst.

Computational Method

All electronic structure calculations have been conducted using the Vienna Ab-initio Simulation Package (VASP) with the projector augmented wave (PAW) method. The generalized gradient approximation method, employing the Perdew-Burke-Ernzerhof (PBE) functional for the

exchange-correlation term, has been utilized. In these calculations, a plane wave basis set with a cutoff energy of 550 eV was utilized. The energy and force convergence criteria have set as 10^{-5} eV and 0.02 eV $Å^{-1}$. A (2 × 2 × 1) mesh has been used for Brillouin zone sampling. The hydrogen adsorption energy is calculated using the following equation:

$$\Delta G_{H*} = \Delta E + \Delta E_{ZPE} - T\Delta S$$

Where ΔE, ΔE_{ZPE} and ΔS are the difference in DFT calculated energy, zero-point energy and entropy between the adsorbed H atom and the gaseous phase H_2.

HER is a two-electron transfer process and the reaction mechanism in acidic medium is as follows:

Volmer: $substrate(*) + H^+ + e^- \rightarrow H^*$

Heyrovsky: $H^* + H^+ + e^- \rightarrow H_2 + substrate\,(*)$

Tafel: $H^* + H^* \rightarrow H_2 + 2\,substrate\,(*)$

The initial stage involves the adsorption of hydrogen ions onto the electrode surface (Volmer step). Following this, there are two possible pathways: either the two hydrogen atoms adsorbed on the surface recombine (Tafel step), or a hydrated proton directly bonds with the adsorbed hydrogen atom, accompanied by electron transfer from the electrode surface (Heyrovsky step).

Single crystal X-ray diffraction

Suitable single crystals were carefully selected under an optical microscope and mounted on thin glass fiber carefully. The single crystal data of both the compounds were collected using Bruker D8-Quest diffractometer. The instrument was equipped with Mo Kα (λ=0.71073Å) radiation

source and operating voltage of X-ray generator was 50 kV and 1 mA. Diffraction data were collected with ω scan width of 0.5º. Three different setting of φ (0, 90, 180º) were used to collect the total 408 frames, keeping a fixed distance of sample-to-detector at 6.03 cm and the detector position (2θ) was fixed at -25º. The initial indexing, final data sets, and cell refinements were handled by an APEX3 program, while a SAINTPLUS[22]program was utilized for the frame integration and final cell parameter calculation. The multi-scan absorption data was corrected by a SADABS program.[23] We initially solved the structure by SIR 92,[24] and the full matrix least-square method (SHELXL-2016[25]) was used further, which is present in the WinGx suit of programs (Version 1.63.04a).[26, 27]) With the help of Fourier maps, we successfully located all the non-hydrogen atoms and refined them anisotropically. Finally, all the hydrogen atoms were fixed at calculated positions and included them in the refinement process using riding model associated with isotropic thermal parameters. The details of the crystal and final refinements are given in the Table S2. CCDC: 2368873 contain the crystallographic data for this paper. These data can be obtained free of charge from The Cambridge Crystallographic Data Center (CCDC) via www.ccdc.cam.ac.uk/data_request/cif.

Table S2: Crystal data and structure refinement parameters for $[Ni_2(NNG)(NA)_3(\mu_2\text{-}H_2O)]$, Ni-MOF.

Empirical formula	$C_{26}H_{21}N_5Ni_2O_{10}$
Formula weight	680.90
Crystal system	Orthorhombic
Space group	*P b c a*
a (Å)	10.0638(8)
b (Å)	20.4928(17)
c (Å)	29.083(2)
α (deg)	90
β (deg)	90
γ (deg)	90
Volume (Å^3)	5997.9(8)
Z	8
T (K)	298(2)
ρcalc (g cm^{-3})	1.508
μ (mm^{-1})	1.317
θ range (deg)	1.988 to 27.118
λ (Mo Kα) (Å)	0.71073
R indices [I>2σ(I)]	$R_1 = 0.0670$, $wR_2 = 0.0856$
R indices (all data)	$R_1 = 0.1130$, $wR_2 = 0.0986$

$R_1 = \Sigma ||F_0|-|F_c|| / \Sigma |F_0|$; $wR_2 = \{\Sigma[w(F_0^2 - F_c^2)^2] / \Sigma[w(F_0^2)^2]^{1/2}$. $w = 1/[\sigma^2(F_0)^2 + (aP)^2 + bP]$, $P = [max.(F_0^2,0) + 2(F_c)^2]/3$, where a = 0.0051 and b = 13.5345

Table S3: Selected bond distances (Å) observed in $[Ni_2(NNG)(NA)_3(\mu_2\text{-}H_2O)]$, Ni-MOF.

Bond	Distances, Å	Bond	Distances, Å
Ni(1)-O(8)#1	2.021(3)	Ni(2)-O(6)	2.005(3)
Ni(1)-O(2)#2	2.030(3)	Ni(2)-O(3)#3	2.036(3)
Ni(1)-O(7)	2.078(3)	Ni(2)-N(3)	2.097(3)
Ni(1)-N(1)	2.082(3)	Ni(2)-O(9)#1	2.101(3)
Ni(1)-O(10)	2.084(3)	Ni(2)-O(10)	2.107(3)
Ni(1)-N(2)	2.123(4)	Ni(2)-N(5)#2	2.132(3)

Symmetry transformations used to generate equivalent atoms: #1 x+1/2, -y+1/2, -z+1 #2 x-1/2, y, -z+3/2 #3 -x, -y, -z+1

Table S4: Selected bond angles observed in $[Ni_2(NNG)(NA)_3(\mu_2\text{-}H_2O)]$, Ni-MOF.

Angle	Amplitude (º)	Angle	Amplitude (º)
O(8)#1-Ni(1)-O(2)#2	174.46(12)	O(6)-Ni(2)-O(3)#3	173.97(13)
O(8)#1-Ni(1)-O(7)	93.96(12)	O(6)-Ni(2)-N(3)	89.72(13)
O(2)#2-Ni(1)-O(7)	88.67(12)	O(3)#3-Ni(2)-N(3)	85.84(13)
O(8)#1-Ni(1)-N(1)	90.97(12)	O(6)-Ni(2)-O(9)#1	91.49(12)
O(2)#2-Ni(1)-N(1)	84.32(12)	O(3)#3-Ni(2)-O(9)#1	84.22(13)
O(7)-Ni(1)-N(1)	86.57(13)	N(3)-Ni(2)-O(9)#1	87.09(13)
O(8)#1-Ni(1)-O(10)	94.09(12)	O(6)-Ni(2)-O(10)	94.90(12)
O(2)#2-Ni(1)-O(10)	90.79(12)	O(3)#3-Ni(2)-O(10)	89.63(13)
O(7)-Ni(1)-O(10)	89.90(13)	N(3)-Ni(2)-O(10)	175.24(13)
N(1)-Ni(1)-O(10)	174.03(13)	O(9)#1-Ni(2)-O(10)	93.92(12)
O(8)#1-Ni(1)-N(2)	87.53(12)	O(6)-Ni(2)-N(5)#2	91.26(13)
O(2)#2-Ni(1)-N(2)	89.69(13)	O(3)#3-Ni(2)-N(5)#2	93.08(13)
O(7)-Ni(1)-N(2)	177.67(13)	N(3)-Ni(2)-N(5)#2	93.49(14)
N(1)-Ni(1)-N(2)	91.62(14)	O(9)#1-Ni(2)-N(5)#2	177.20(14)
O(10)-Ni(1)-N(2)	91.77(14)	O(10)-Ni(2)-N(5)#2	85.28(13)

Symmetry transformations used to generate equivalent atoms: #1 x+1/2,-y+1/2,-z+1 #2 x-1/2,y,-z+3/2 #3 -x,-y,-z+1

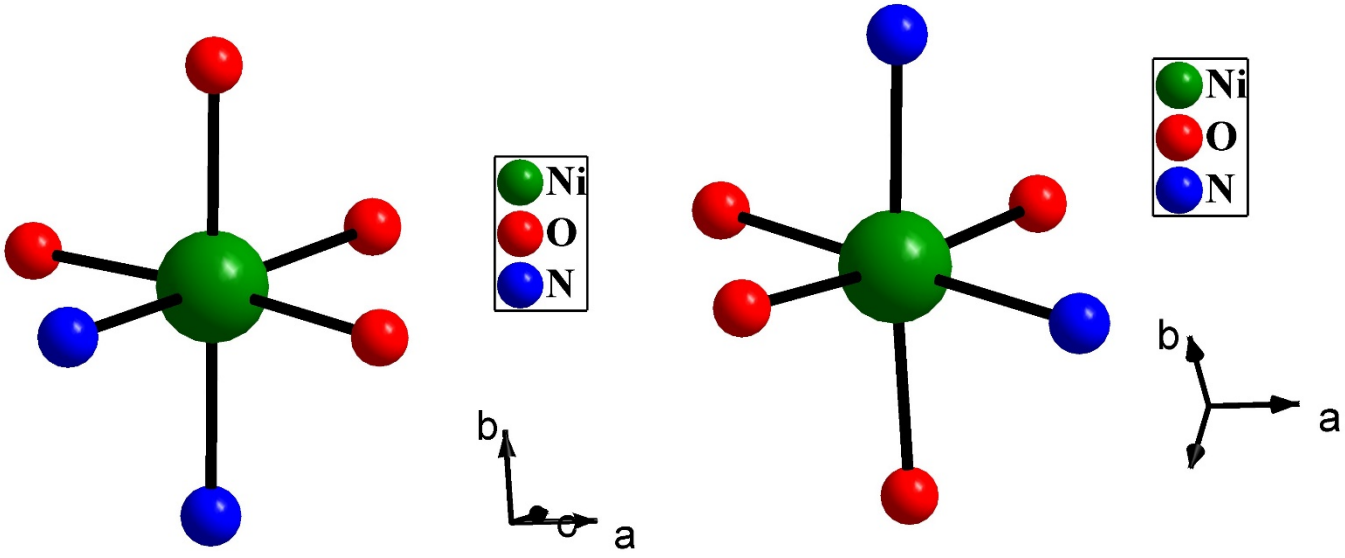

Fig. S1: Octahedral geometry around Ni ions in Ni-MOF (a) around $Ni(1)^{2+}$ ion, (b) around $Ni(2)^{2+}$ ion.

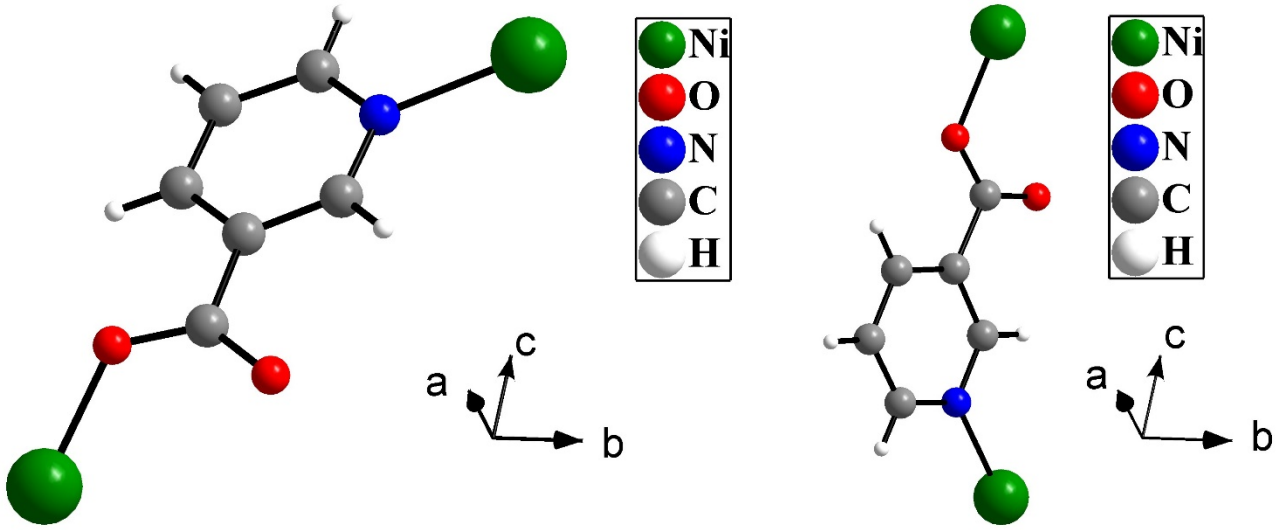

Fig. S2: Monodentate connectivity of NA in Ni-MOF (a) NA1 and (b) NA2.

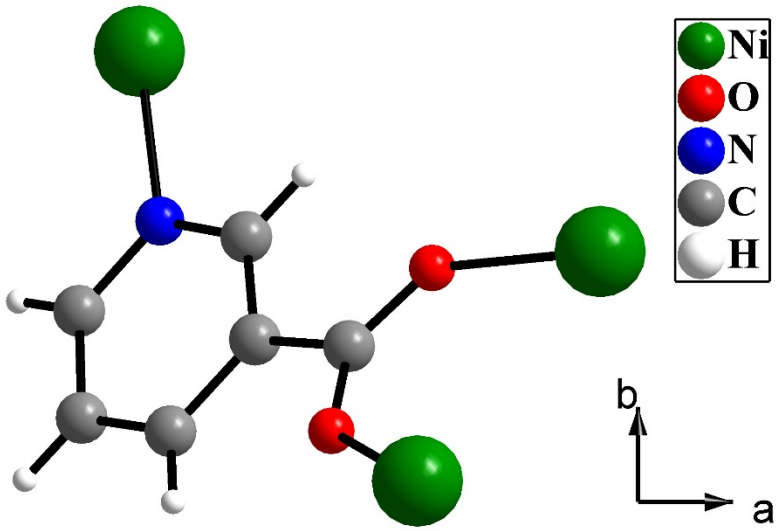

Fig. S3a: Bidentate connectivity of NA3 in Ni-MOF.

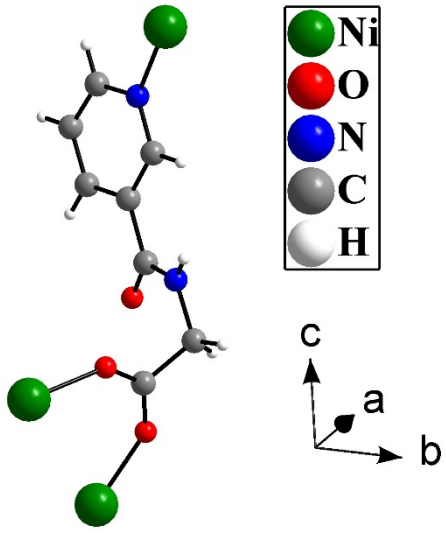

Fig. S3b: Bidentate connectivity of N-NG in Ni-MOF.

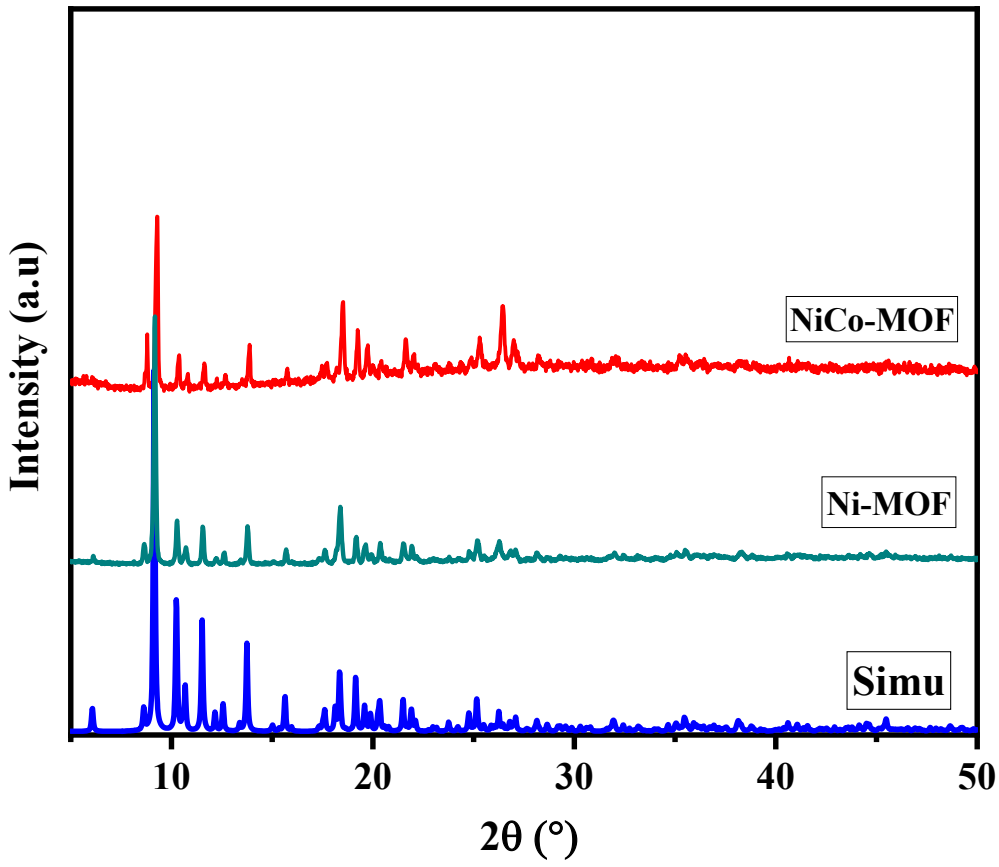

Fig. S4: Powder XRD (CuKα) patterns of Ni-MOF and NiCo-MOF.

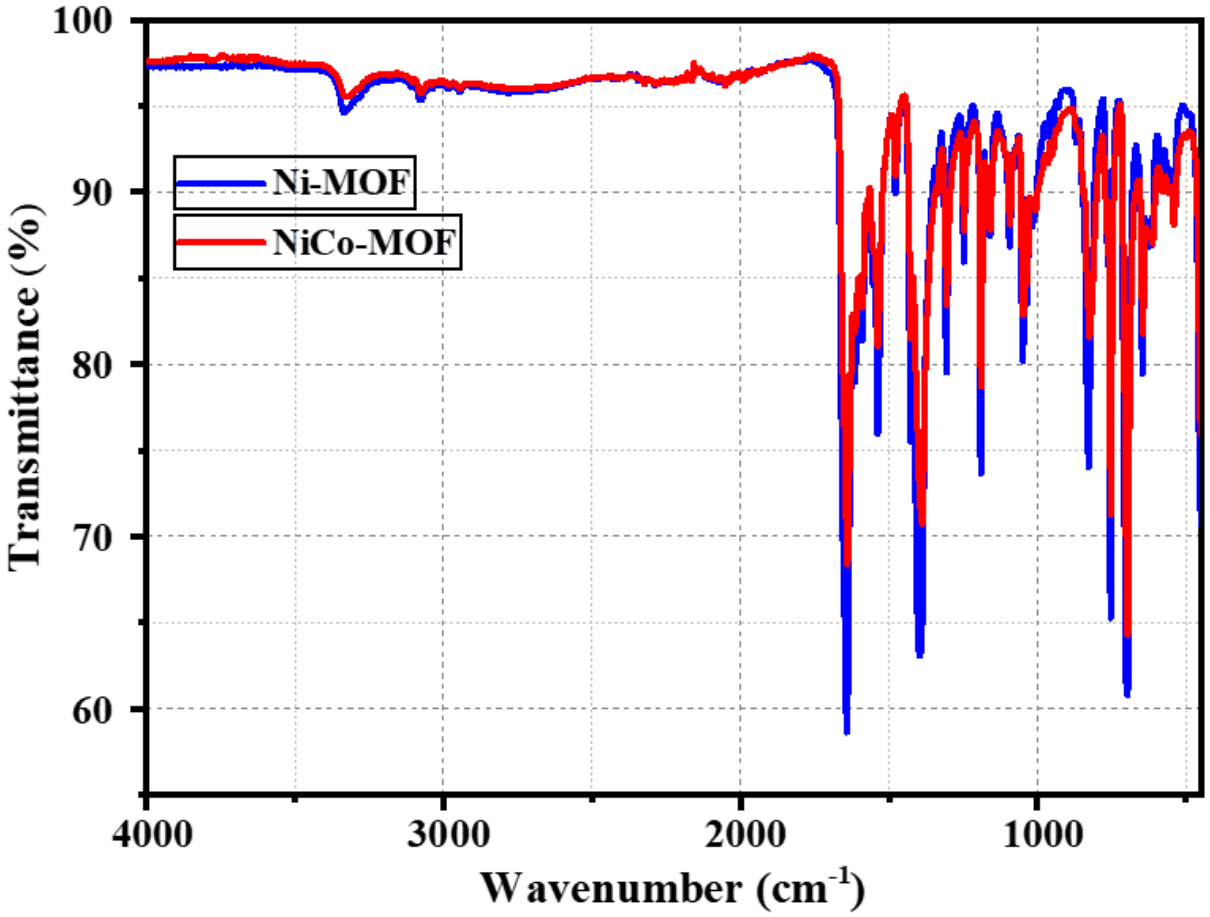

Fig. S5: IR spectra Ni-MOF and NiCo-MOF.

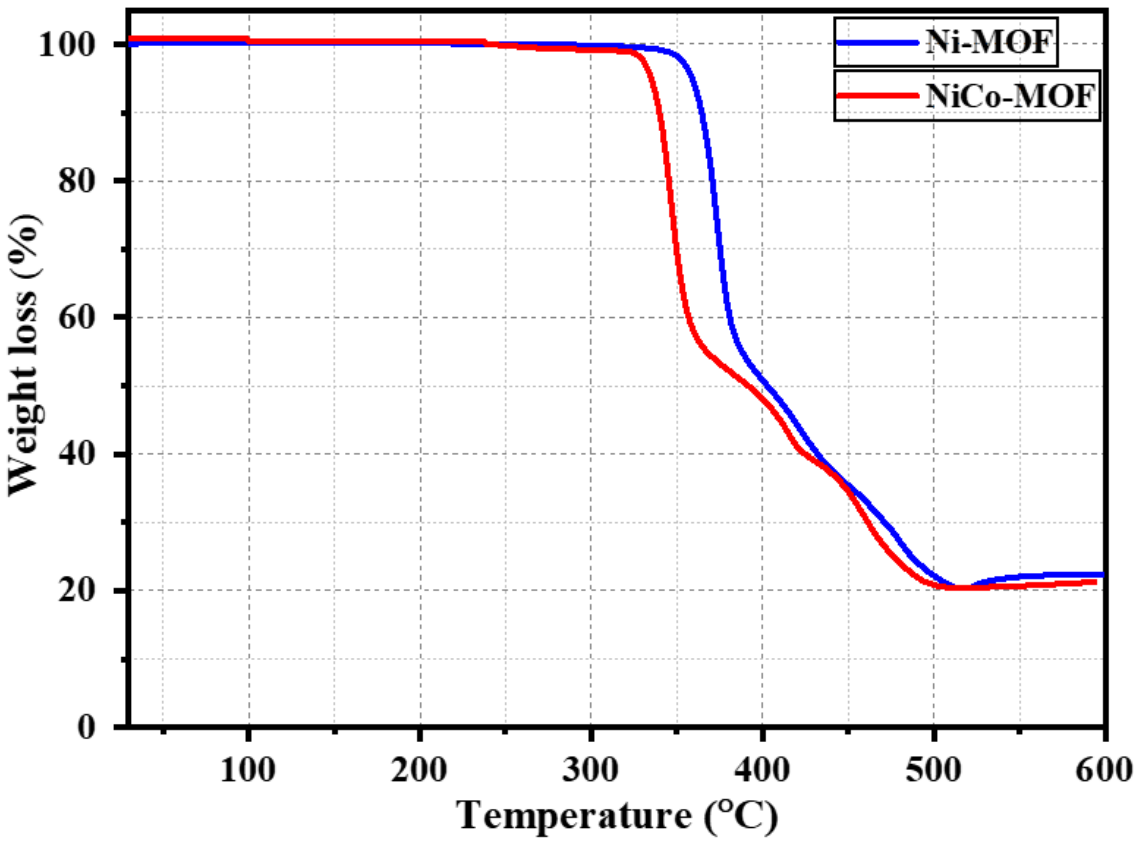

Fig. S6: Thermogravimetric analysis (TGA) of Ni-MOF and NiCo-MOF in nitrogen atmosphere.

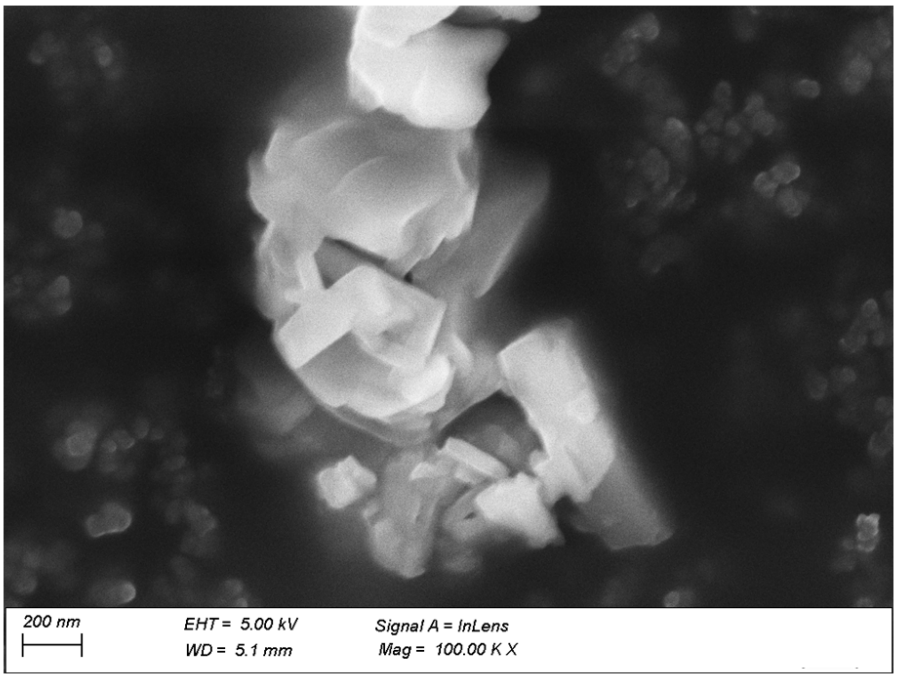

Fig. S7a: SEM image of Ni-MOF.

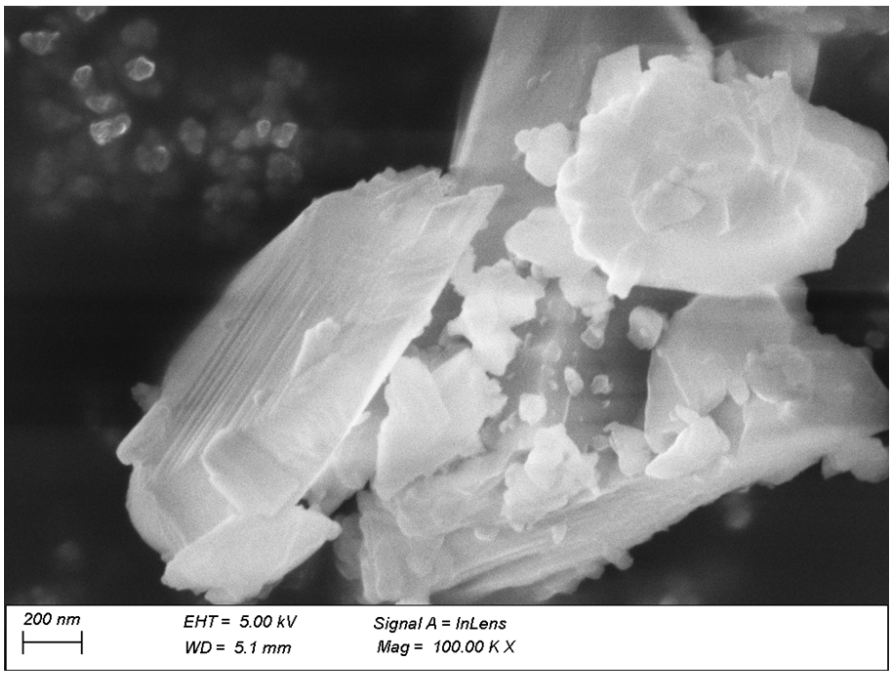

Fig. S7b: SEM image of NiCo-MOF.

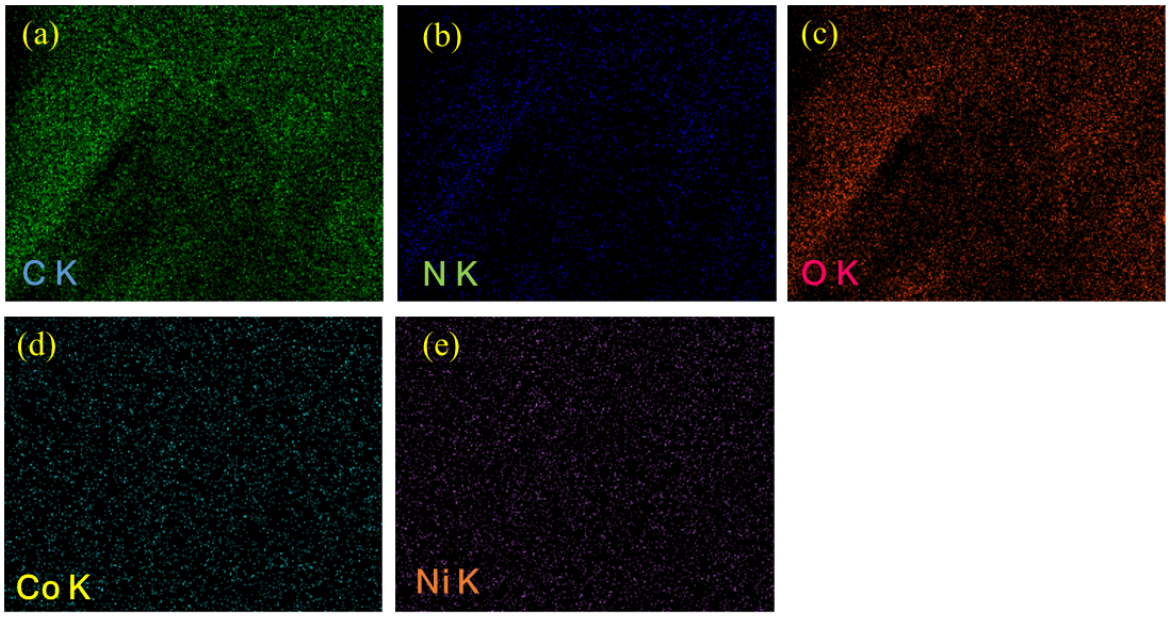

Fig. S8: Elemental mapping images of NiCo-MOF for (a) C-K and (b) N-K, (c) O-K (d) Co-K and (e) Ni-K.

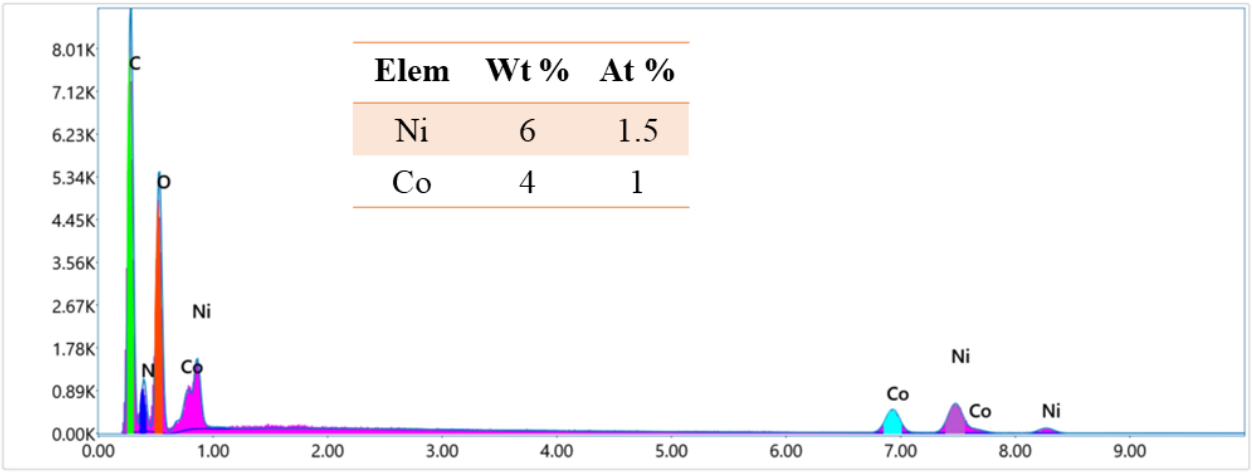

Fig. S9: Representative EDX plot of NiCo-MOF. Note the presence of Ni and Co.

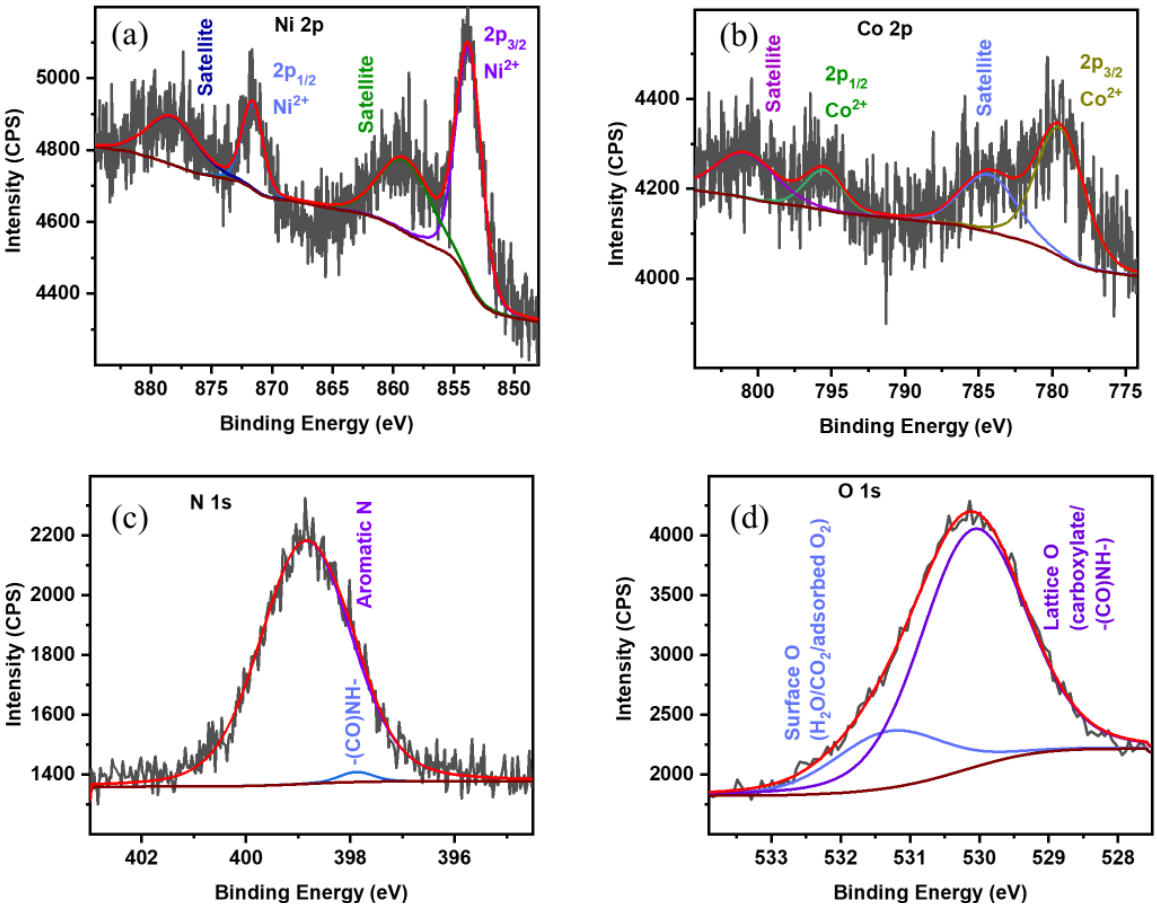

Fig. S10: High resolution XPS spectra of (a) Ni 2p, (b) Co 2p, (c) N 1s, and (d) O 1s of NiCo-MOF.

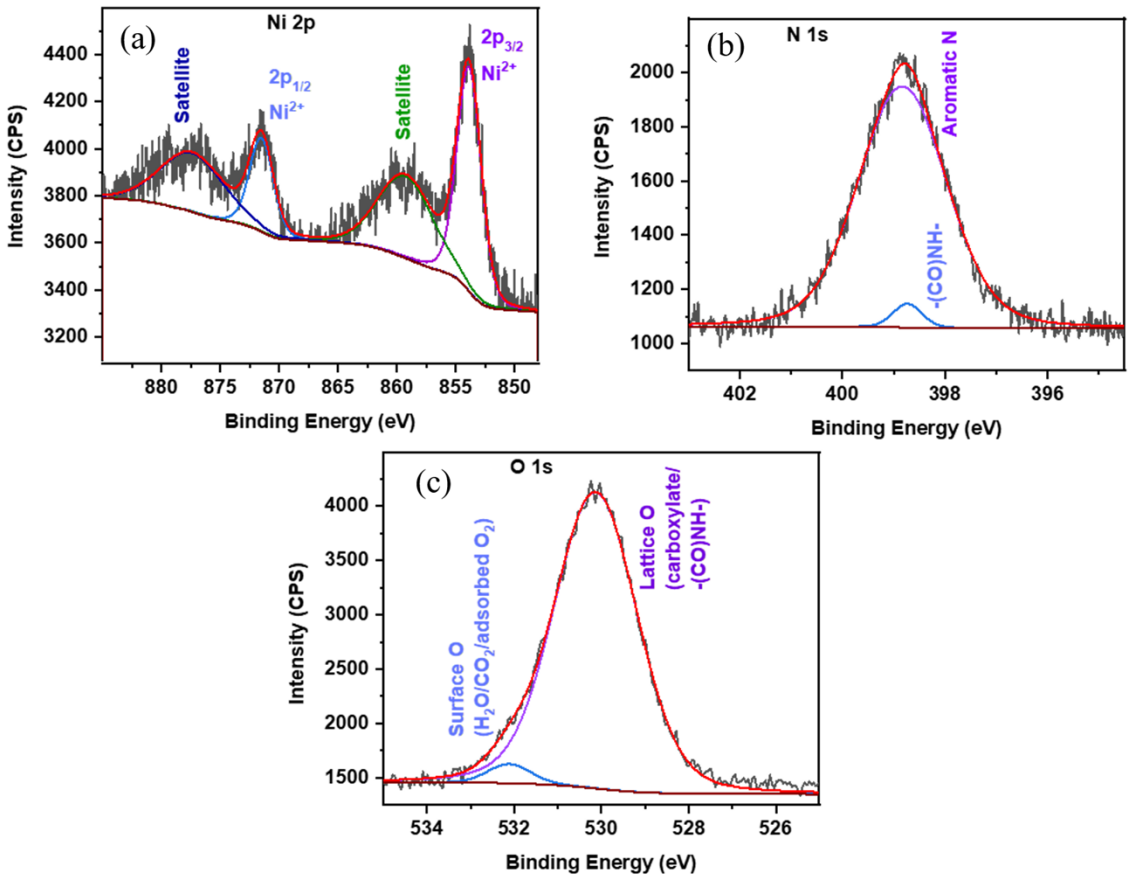

Fig. S11: High resolution XPS spectra of (a) Ni 2p, (b) N 1s, and (c) O 1s of Ni-MOF.

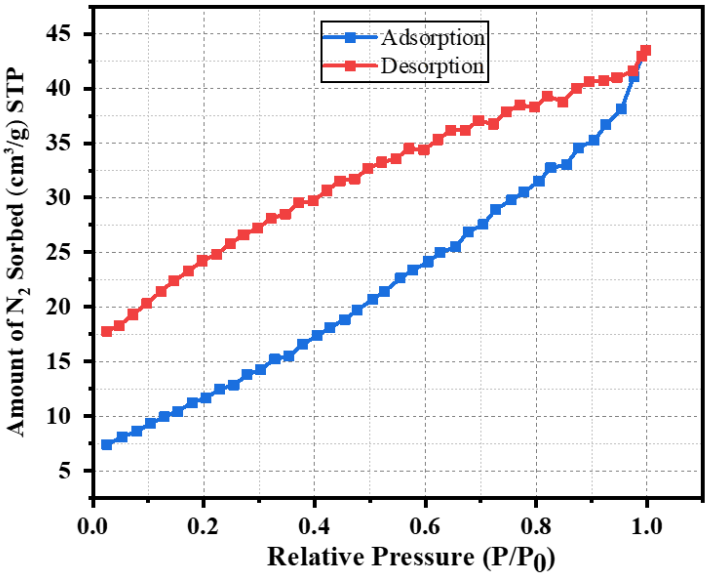

Fig. S12: N_2 adsorption (at 77 K) isotherms of Ni-MOF, blue represents the adsorption and red represents desorption. The obtained correlation coefficient (R^2) value is 0.997 and C value is 48.37.

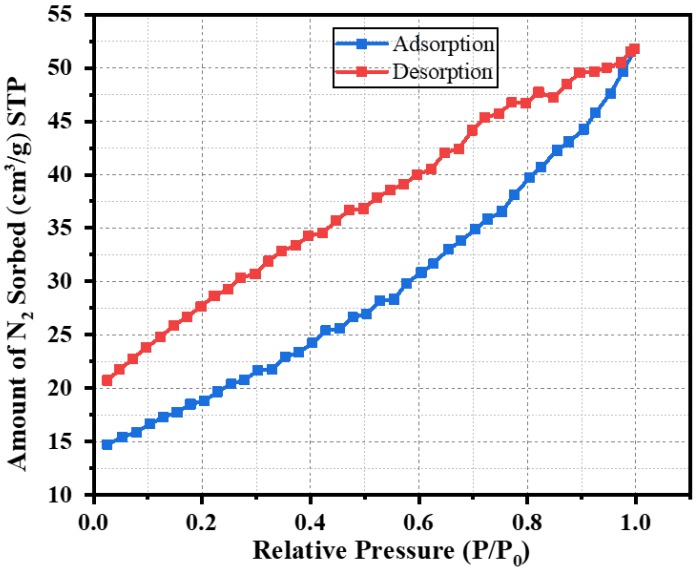

Fig. S13: N_2 adsorption (at 77 K) isotherms of NiCo-MOF, blue represents the adsorption and red represents desorption. The obtained correlation coefficient (R^2) value is 0.999 and C value is 459.62.

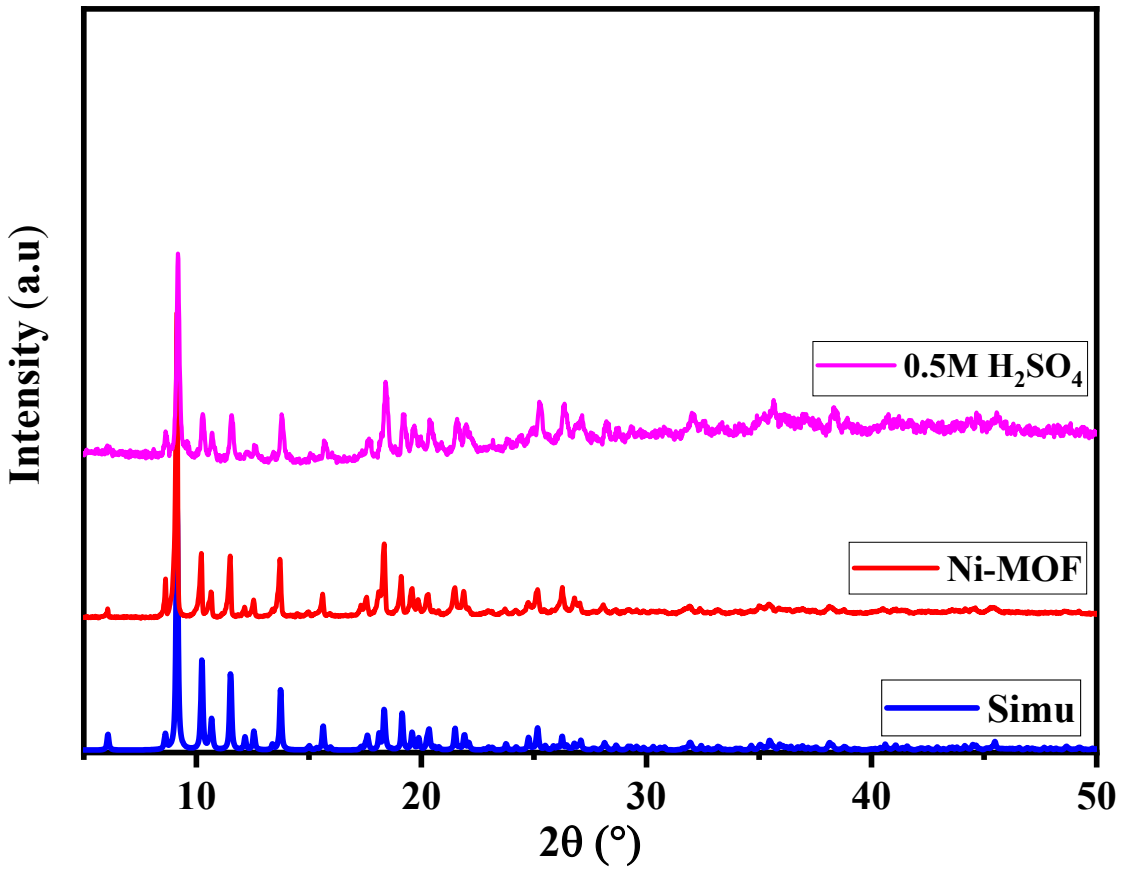

Fig. S14: Powder XRD (CuKα) patterns of Ni-MOF after six hours acid treatment.

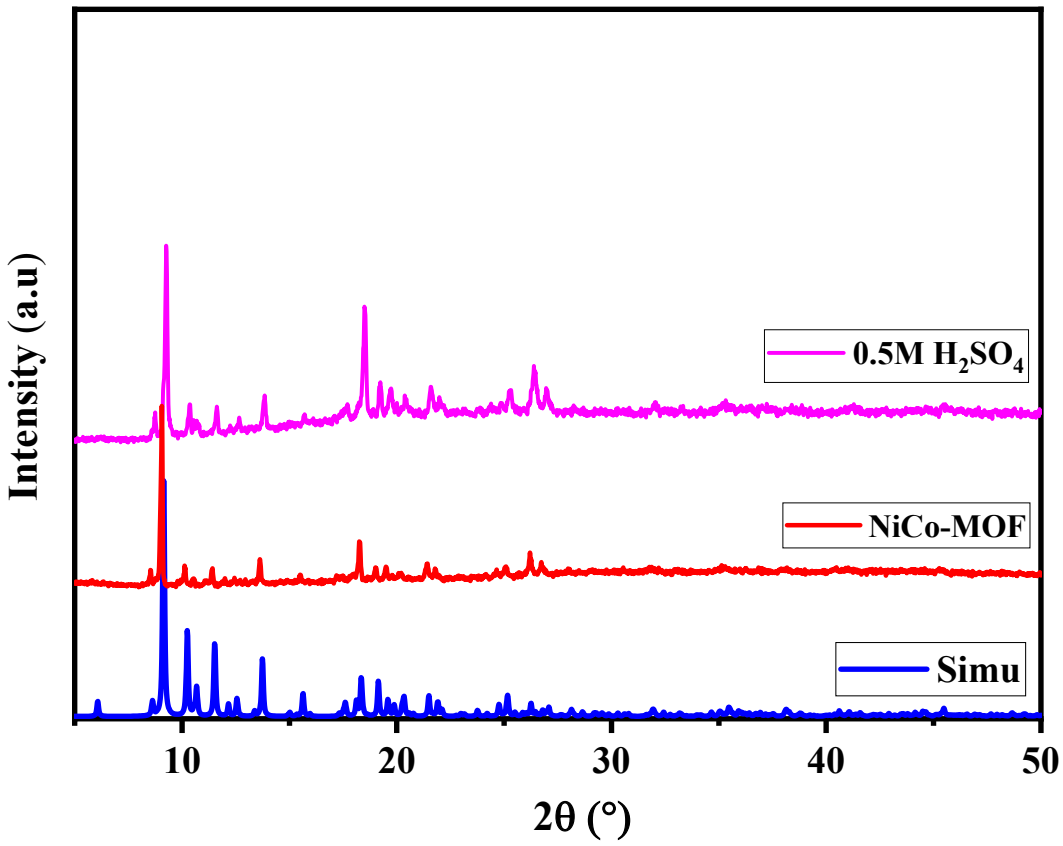

Fig. S15: Powder XRD (CuKα) patterns of NiCo-MOF after six hours acid treatment.

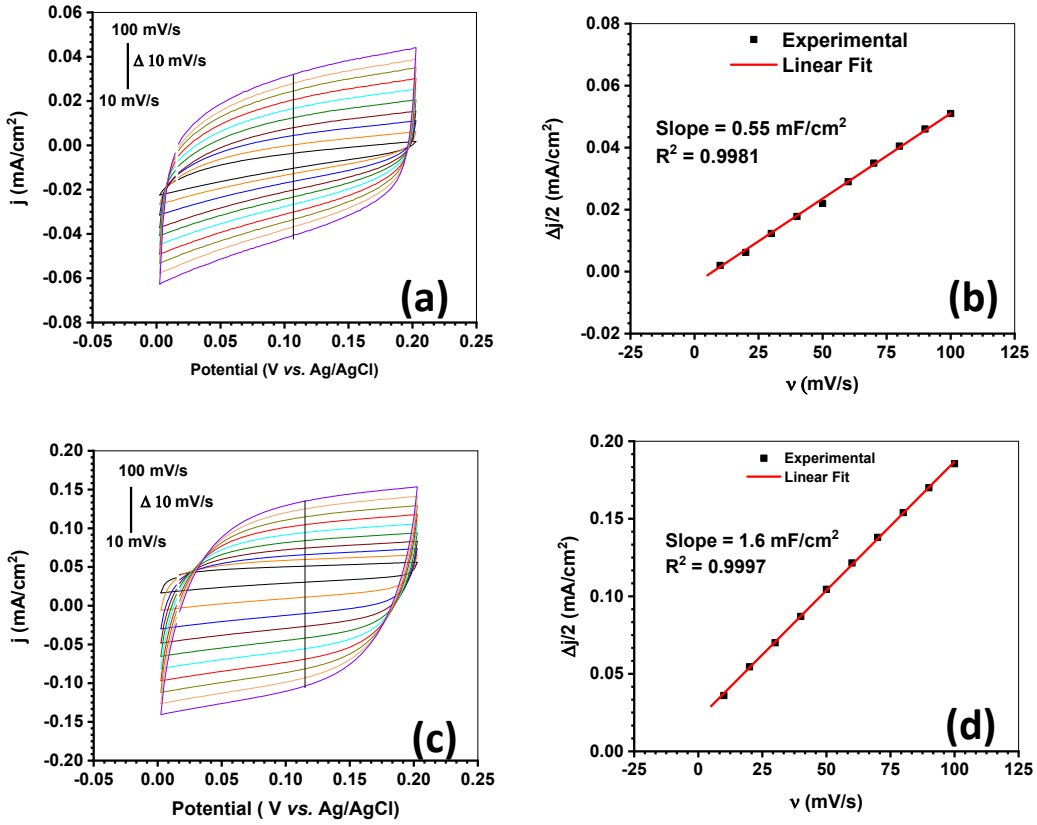

Fig. S16: CV profiles at variable scan rate (υ) within the voltage range of non-Faradaic current response: (a) Ni-MOF & (c) NiCo-MOF; and Estimation of double layer capacitance from the linear fitting of Δj/2 *vs*. υ profiles: (b) Ni-MOF & (d) NiCo-MOF.

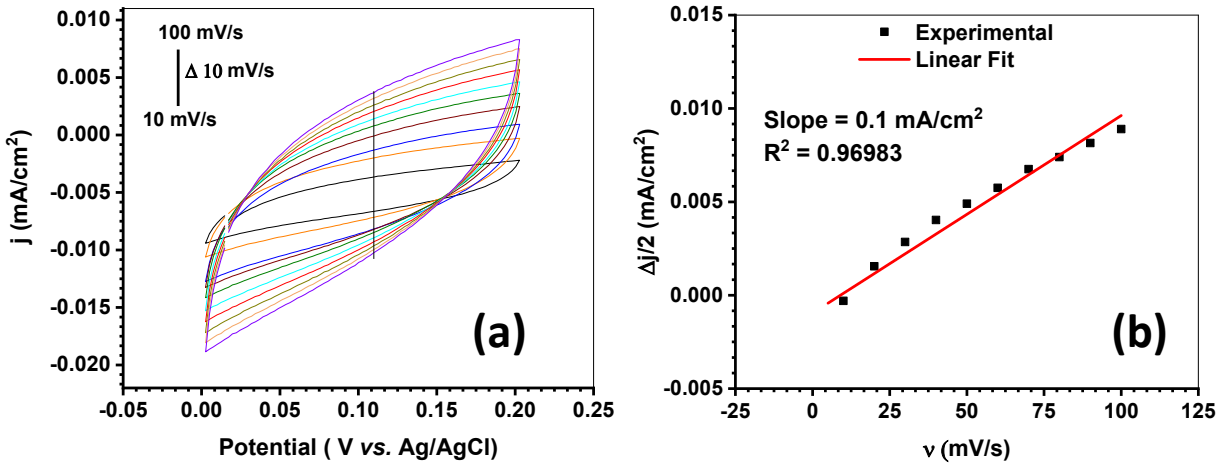

Fig. S17**:** (a) CV profiles for blank electrode at variable scan rate (υ), and (b) estimation of double layer capacitance of blank electrode (C_s) from the linear fitting of Δj/2 *vs*. υ profile.

Calculations of Faradaic Efficiency.

To determine the Faradaic efficiency of MOF-based catalysts for the HER, we performed additional experiments using a two-electrode configuration. A H-type, two-compartment glass electrochemical cell was employed, wherein stainless steel electrode (2 × 2 cm^2) coated with the MOF catalysts served as the cathode, and a platinum mesh was used as the anode for the OER. The electrolyte used in both compartments was 0.5 M H_2SO_4. Hydrogen gas generated at the cathode was collected via the downward displacement of water in an inverted burette setup. Chronopotentiometric measurements were conducted at a constant current density of 10 mA cm^{-2} for 1 hour. The theoretical amount of hydrogen evolved was calculated using the following equation:

Theoretical H_2 evolution (mol) = (I × t) / (n × F)

where I is the applied current (A), t is the time (s), F is the Faraday constant (96,485 C mol^{-1}), and n = 2 for HER.

The Faradaic efficiency was determined using:

Faradaic Efficiency (%) = (Experimental H_2 evolved / Theoretical H_2 evolved) × 100 %

Under the experimental conditions, the volumes of hydrogen collected were 15.0 mL for NiCo-MOF and 14.5 mL for Ni-MOF, compared to a theoretical evolution of 16.7 mL. Based on these values, the Faradaic efficiencies were calculated to be 90.4% and 86.8% for NiCo-MOF and Ni-MOF, respectively, confirming the better catalytic performance and efficiency of bimetallic NiCo-MOF.

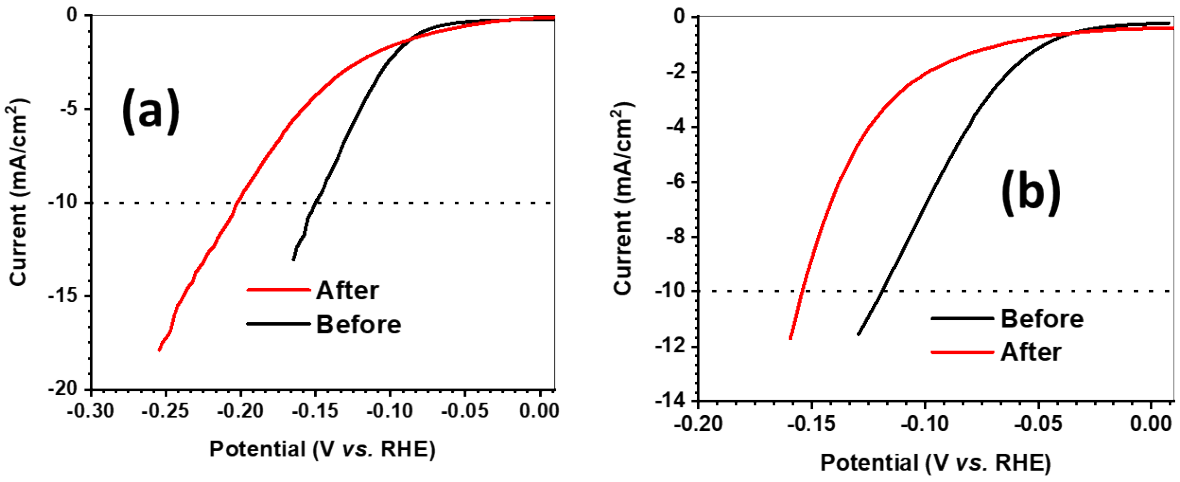

Fig. S18: Durability study through CV cycling: Comparative LSV profiles for (a) Ni-MOF & (b) NiCo-MOF.

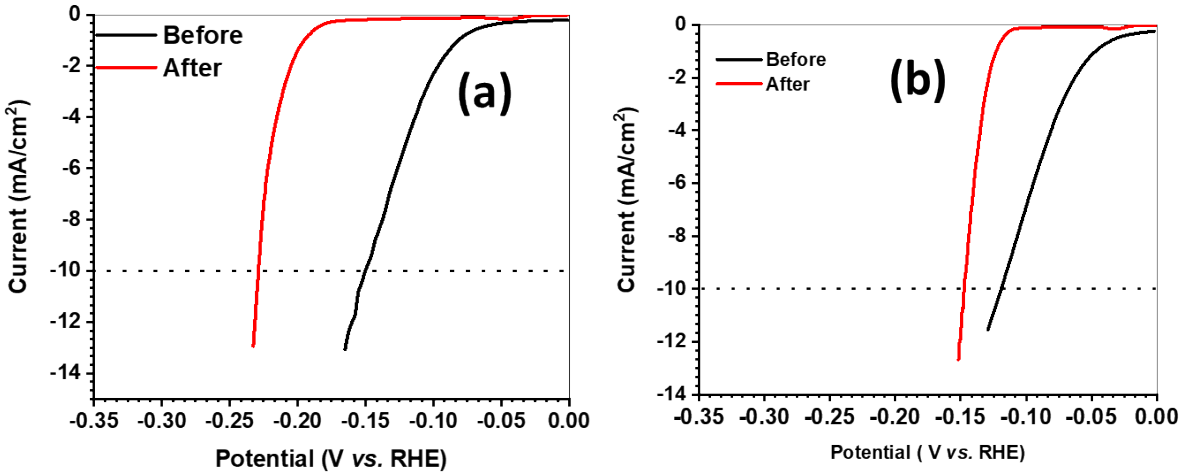

Fig. S19: Durability study through Chronoamperometry: Comparative LSV profiles before and after durability test for (a) Ni-MOF & (b) NiCo-MOF.

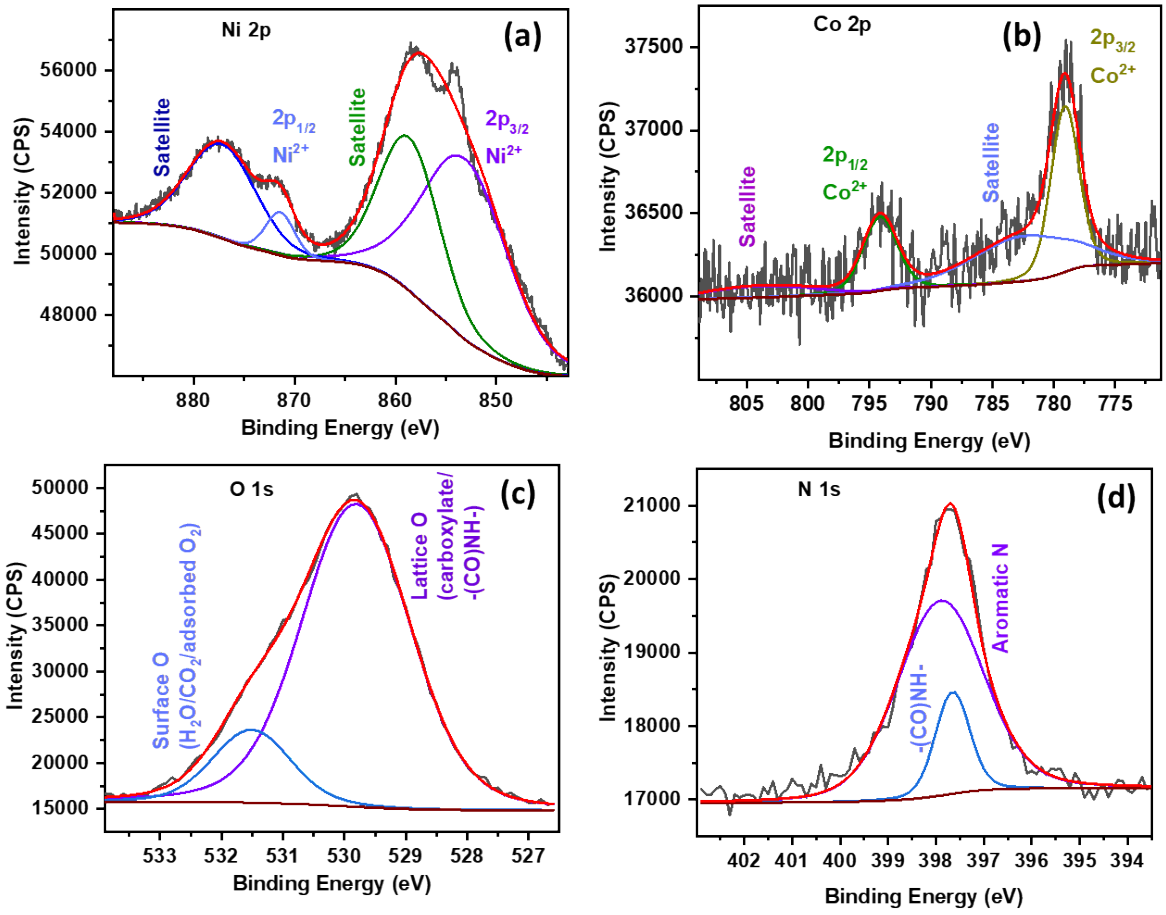
Ni 2p
(a)
Satellite
2p1/2
Ni2+
Satellite
2p3/2
Ni2+
Intensity (CPS)
Binding Energy (eV)
Co 2p
(b)
2p3/2
Co2+
2p1/2
Co2+
Satellite
Satellite
Intensity (CPS)
Binding Energy (eV)
O 1s
(c)
Surface O
(H2O/CO2/adsorbed O2)
Lattice O
(carboxylate/
-(CO)NH-)
Intensity (CPS)
Binding Energy (eV)
N 1s
(d)
Aromatic N
-(CO)NH-
Intensity (CPS)
Binding Energy (eV)

Fig. S20: Post-Experiment XPS analysis of NiCo-MOF: (a) Ni 2p, (b) Co 2p, (c) O 1s and (d) N 1s.

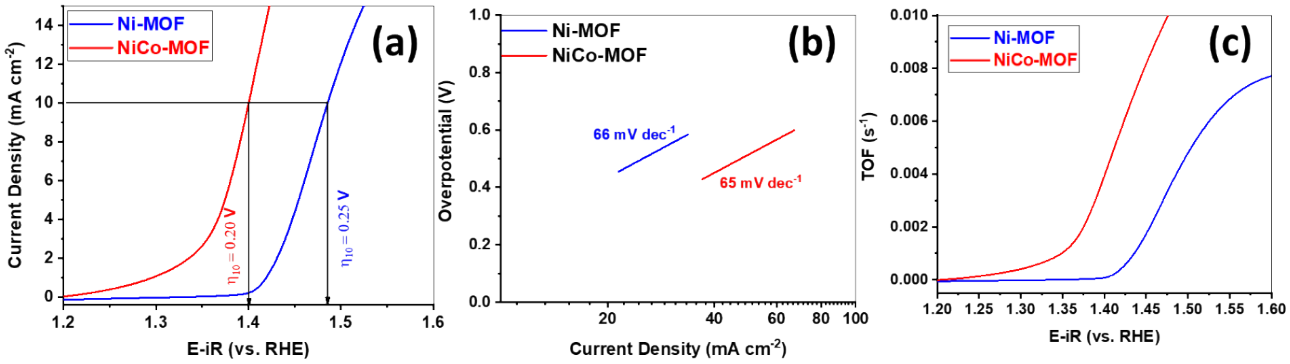

Fig. S21: OER activity of the MOFs: (a) Linear sweep voltammetry (LSV) profiles indicating η_{10} values, (b) Tafel slopes and (c) TOF profiles.

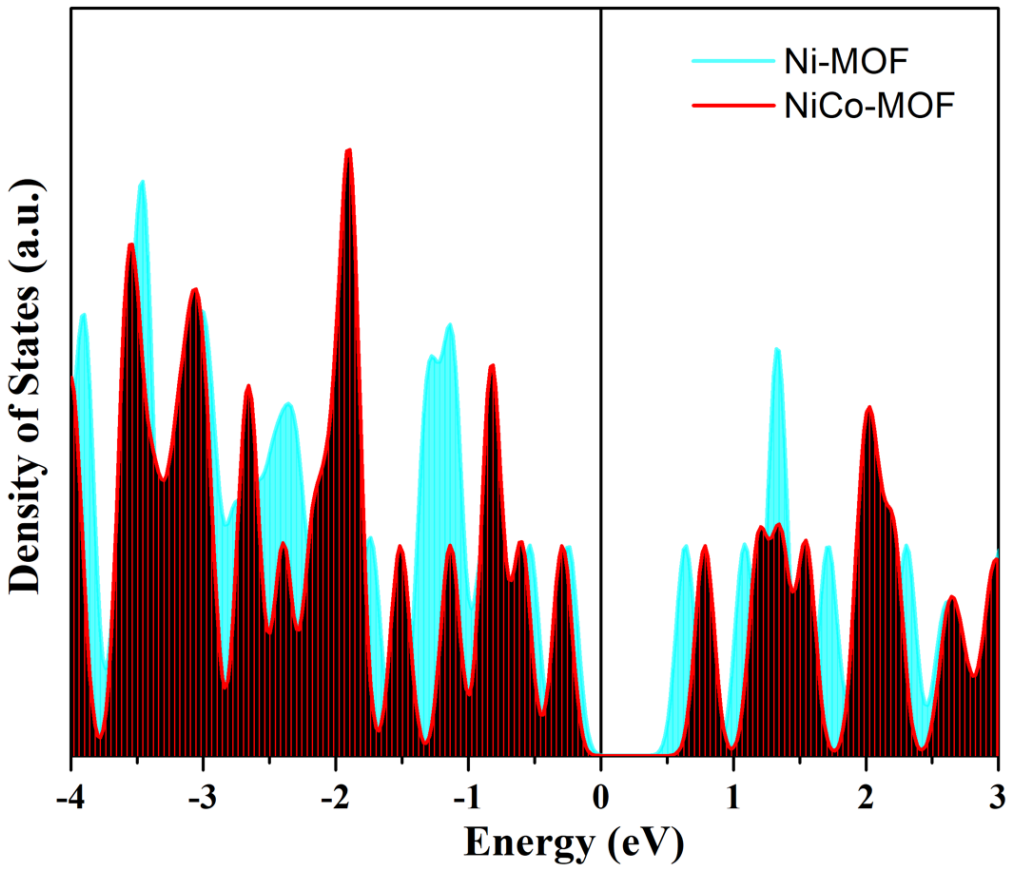

Fig. S22. Total density of states for Ni-MOF and NiCo-MOF.

References

1. J.-S. Qin, D.-Y. Du, W. Guan, X.-J. Bo, Y.-F. Li, L.-P. Guo, Z.-M. Su, Y.-Y. Wang, Y.-Q. Lan and H.-C. Zhou, *Journal of the American Chemical Society*, 2015, **137**, 7169-7177.
2. R. Dong, Z. Zheng, D. C. Tranca, J. Zhang, N. Chandrasekhar, S. Liu, X. Zhuang, G. Seifert and X. Feng, *Chemistry – A European Journal*, 2017, **23**, 2255-2260.
3. R. Dong, M. Pfeffermann, H. Liang, Z. Zheng, X. Zhu, J. Zhang and X. Feng, *Angewandte Chemie International Edition*, 2015, **54**, 12058-12063.
4. Y.-P. Wu, W. Zhou, J. Zhao, W.-W. Dong, Y.-Q. Lan, D.-S. Li, C. Sun and X. Bu, *Angewandte Chemie International Edition*, 2017, **56**, 13001-13005.
5. L. Zhang, S. Li, C. J. Gómez-García, H. Ma, C. Zhang, H. Pang and B. Li, *ACS Applied Materials & Interfaces*, 2018, **10**, 31498-31504.
6. I. Hod, P. Deria, W. Bury, J. E. Mondloch, C.-W. Kung, M. So, M. D. Sampson, A. W. Peters, C. P. Kubiak, O. K. Farha and J. T. Hupp, *Nature Communications*, 2015, **6**, 8304.
7. H. Huang, Y. Zhao, Y. Bai, F. Li, Y. Zhang and Y. Chen, *Advanced Science*, 2020, **7**, 2000012.
8. V. Khrizanforova, R. Shekurov, V. Miluykov, M. Khrizanforov, V. Bon, S. Kaskel, A. Gubaidullin, O. Sinyashin and Y. Budnikova, *Dalton Transactions*, 2020, **49**, 2794-2802.
9. R. Shekurov, V. Khrizanforova, L. Gilmanova, M. Khrizanforov, V. Miluykov, O. Kataeva, Z. Yamaleeva, T. Burganov, T. Gerasimova, A. Khamatgalimov, S. Katsyuba, V. Kovalenko, Y. Krupskaya, V. Kataev, B. Büchner, V. Bon, I. Senkovska, S. Kaskel, A. Gubaidullin, O. Sinyashin and Y. Budnikova, *Dalton Transactions*, 2019, **48**, 3601-3609.
10. S. Roy, Z. Huang, A. Bhunia, A. Castner, A. K. Gupta, X. Zou and S. Ott, *Journal of the American Chemical Society*, 2019, **141**, 15942-15950.
11. A. J. Clough, J. W. Yoo, M. H. Mecklenburg and S. C. Marinescu, *Journal of the American Chemical Society*, 2015, **137**, 118-121.
12. D. Micheroni, G. Lan and W. Lin, *Journal of the American Chemical Society*, 2018, **140**, 15591-15595.
13. A. Hu, Q. Pang, C. Tang, J. Bao, H. Liu, K. Ba, S. Xie, J. Chen, J. Chen, Y. Yue, Y. Tang, Q. Li and Z. Sun, *Journal of the American Chemical Society*, 2019, **141**, 11322-11327.
14. X.-F. Li, M.-Y. Lu, H.-Y. Yu, T.-H. Zhang, J. Liu, J.-H. Tian and R. Yang, *ChemElectroChem*, 2019, **6**, 4507-4510.
15. X. Dai, M. Liu, Z. Li, A. Jin, Y. Ma, X. Huang, H. Sun, H. Wang and X. Zhang, *The Journal of Physical Chemistry C*, 2016, **120**, 12539-12548.
16. H. B. Wu, B. Y. Xia, L. Yu, X.-Y. Yu and X. W. Lou, *Nature Communications*, 2015, **6**, 6512.
17. R.-Z. Zhang, L.-L. Lu, Z.-H. Chen, X. Zhang, B.-Y. Wu, W. Shi and P. Cheng, *Chemistry – A European Journal*, 2022, **28**, e202200401.
18. K. Chen, D. Ray, M. E. Ziebel, C. A. Gaggioli, L. Gagliardi and S. C. Marinescu, *ACS Applied Materials & Interfaces*, 2021, **13**, 34419-34427.
19. Y. Xie, J. Cai, Y. Wu, Y. Zang, X. Zheng, J. Ye, P. Cui, S. Niu, Y. Liu, J. Zhu, X. Liu, G. Wang and Y. Qian, *Advanced Materials*, 2019, **31**, 1807780.

20. A. Govind Rajan, J. M. P. Martirez and E. A. Carter, *ACS Catalysis*, 2020, **10**, 11177-11234.
21. L. R. F. A. J. Bard, ed., *Electrochemical Methods. Fundamentals and Applications*, Wiley, New York, 2001.
22. *Apex3 v2017.3-0*, *Saint V8.38A*, *SAINT V8.38A*; Bruker AXS Inc.: Madison, WI, 2018.
23. L. Krause, R. Herbst-Irmer, G. M. Sheldrick and D. Stalke, *Journal of Applied Crystallography*, 2015, **48**, 3-10.
24. A. Altomare, G. Cascarano, C. Giacovazzo and A. Guagliardi, *Journal of Applied Crystallography*, 1993, **26**, 343-350.
25. G. M. J. A. C. S. C. S. C. Sheldrick, 2015, **71**, 3-8.
26. L. Farrugia, *Journal of Applied Crystallography*, 1999, **32**, 837-838.
27. A. Spek, *Journal of Applied Crystallography*, 2003, **36**, 7-13.